SCIENTIFIC REPORTS

OPEN

Klein tunneling in Weyl semimetals under the influence of magnetic field

Can Yesilyurt[1], Seng Ghee Tan[1,2], Gengchiau Liang[1] & Mansoor B. A. Jalil[1]

Klein tunneling refers to the absence of normal backscattering of electrons even under the case of high potential barriers. At the barrier interface, the perfect matching of electron and hole wavefunctions enables a unit transmission probability for normally incident electrons. It is theoretically and experimentally well understood in two-dimensional relativistic materials such as graphene. Here we investigate the Klein tunneling effect in Weyl semimetals under the influence of magnetic field induced by ferromagnetic stripes placed at barrier boundaries. Our results show that the resonance of Fermi wave vector at specific barrier lengths gives rise to perfect transmission rings, i.e., three-dimensional analogue of the so-called magic transmission angles in two-dimensional Dirac semimetals. Besides, the transmission profile can be shifted by application of magnetic field in the central region, a property which may be utilized in electro-optic applications. When the applied potential is close to the Fermi level, a particular incident vector can be selected by tuning the magnetic field, thus enabling highly selective transmission of electrons in the bulk of Weyl semimetals. Our analytical and numerical calculations obtained by considering Dirac electrons in three regions and using experimentally feasible parameters can pave the way for relativistic tunneling applications in Weyl semimetals.

Klein paradox, which constitutes one of the most interesting consequences of quantum electrodynamics, has been theoretically predicted for massive particles[1–6]. However, the requirement of very high potential drop makes the observation impossible since the potential barrier height must exceed the rest energy of electrons, i.e., mc^2 (m being the mass of electron and c the speed of light). The discovery of graphene[7] has enabled the experimental realization of this effect in an accessible condensed matter system, since the effective mass of electrons on graphene is zero, which leads to a zero energy gap between electron and hole states. Therefore, even at low applied potential of <1 V, electron and hole wavefunctions can be made to match across the barrier, resulting in signature of Klein tunneling, i.e. unit transmission probability at normal incidence[8]. So far, many works have been done to observe the absence of backscattering under an applied potential in graphene[9,10]. In addition, the so-called magic transmission angles caused by the resonance of Fermi wave vector have been investigated in two-dimensional Dirac semimetals such as graphene[11–13]. Additionally, it is important to analyze the Klein tunneling system under magnetic field since only the phase shift in conductance resonances of a ballistic graphene p-n junction may lead a direct evidence of absence of backscattering at the barrier interface[10,14]. Therefore, it is a prerequisite that any candidate material for Klein tunneling must be analytically treated under the influence of magnetic field as well.

The recent discoveries[15–17] of material systems exhibiting Weyl semimetallic properties have created a viable avenue for realizing three-dimensional relativistic electron transport. In such materials, the so-called Weyl fermions show gapless energy-momentum relation like graphene, but in all three dimensions in k-space. The intriguing nature of Weyl semimetal provides a stable topological state whose low energy dispersion is described by the Weyl Hamiltonian shown in Eq. 1. The Weyl nodes in the bulk of the material always come together in pairs with opposite chirality, carried by the sign of the velocity. This pair of bulk Weyl nodes are connected to one another by the Fermi arc states occurring on the surface. Theoretically, the low energy Hamiltonian of such a system is robust against perturbations since it includes all three Pauli matrices[18]. The exotic features of Weyl semimetals including Weyl nodes in the bulk and Fermi arcs on the surfaces have attracted attention both theoretically and experimentally[19–21]. The surface states (Fermi arcs) have been observed in topological metal[16], TaP[21] and YbMnBi[22] recently. The bulk

[1]Electrical and Computer Engineering, National University of Singapore, Singapore 117576, Republic of Singapore. [2]Data Storage Institute, Agency of Science, Technology and Research (A* Star), Singapore 138634, Republic of Singapore. Correspondence and requests for materials should be addressed to C.Y. (email: can--yesilyurt@hotmail.com) or M.B.A.J. (email: elembaj@nus.edu.sg)
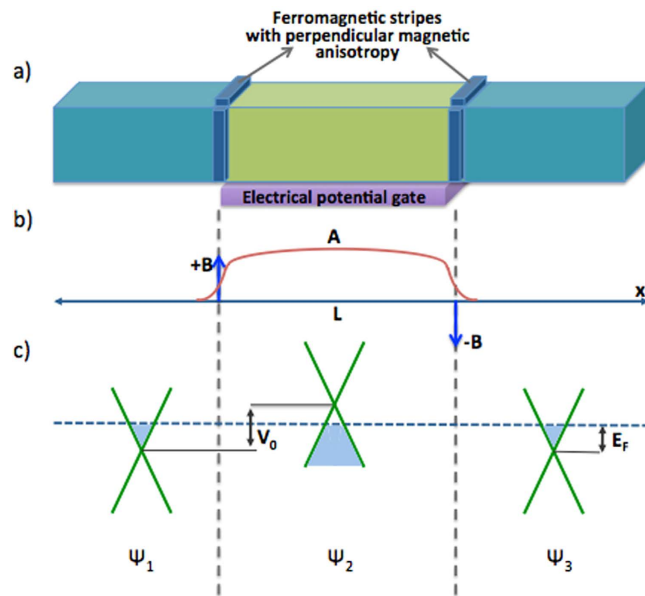
Figure 1. The schematic representation of the single potential barrier Weyl semimetal under the influence of magnetic field induced by four ferromagnetic stripes on the top and one side surfaces. The anti-symmetric anisotropy of ferromagnetic stripes generates a delta function magnetic field **B** thus a magnetic vector potential **A**. Induced potential barrier changes the carrier concentration of barrier region, such that the Fermi level (blue dashed line) cuts across the conduction band in first and third regions, but lies within the valance band in the second region. The occupied states are shown by light blue near the Weyl nodes.

transport properties have also been investigated, and experimental works have shown consistent agreement with theoretical predictions[22–24]. Moreover, due to the high mobility and chiral nature of electrons in Weyl semimetals, they are expected to be ideal candidates for transport and tunneling applications. Several transport applications such as charge transport[25], magnetotransport[26], extremely large magnetoresistance and ultrahigh mobility[27] have been predicted and observed recently.

In this work, we have investigated the properties of Klein tunneling transmission of Weyl fermions (including the so-called "magic" transmission angles) with and without the influence of magnetic fields, which are induced by four ferromagnetic stripes, as shown in Fig. 1. Our tunneling calculations based on electron wave functions in three regions show absence of backscattering for normally incident electrons in the presence of applied gate potential close to Fermi level. Also, we show that a particular wave vector can be selected by tuning the external magnetic fields, which may be useful for electro-optic applications. By calculating the angular dependence of electron transmission, we find that the resonance of Fermi wave vector and the barrier length causes magic transmission rings, i.e., perfect transmission angles in two transverse dimensions where the transmission probability (T) is 1.

Methods

To obtain the transmission probability of the system, we consider electron wavefunctions in the three regions shown, i.e., Ψ_1, Ψ_2 and Ψ_3 for incident, propagated and transmitted electrons, respectively. It is experimentally shown that in three-dimensional Dirac semimetals, the Fermi level as well as potential barrier height, can be tuned by applying a bias to a gated region or by alkali metal doping[28,29]. By modulating the concentrations of alkali metal dopants in the different regions, one can create Weyl semimetal system with a band-profile as shown in Fig. 1(c). Another alternative would be to apply a back gate to all three regions, and one additional top gate to change carrier concentration only within the barrier region, as was demonstrated in ref. 28 in thin-film Dirac semimetal Cd_3As_2 experimentally. However, the fabricated material must be quite thin (several nanometer thickness) since screening effect is only available for short ranges. As shown in Fig. 1, the application of gated potential or metal doping raises the carrier concentration in the barrier region. We assumed a rectangular potential barrier in the central region. If the potential barrier height exceeds the Fermi energy, then the Fermi level will lie within the conduction band in the first and third regions, but cuts across the valence band in the second region. In our scheme, ferromagnetic stripes are placed on top and one side of the Weyl semimetal at the barrier boundaries. The anti-symmetric configuration of ferromagnetic stripes whose magnetic moment perpendicular to the surface induce a localized magnetic field **B** which is modelled by a delta-function at the boundaries. This translates into a magnetic vector potential **A** whose spatial profile is shown in Fig. 1(b). The top and side ferromagnetic stripes create a gauge potential on y- and z-axis respectively. Note that, by controlling the two magnetic fields along y- and z- direction independently, the effective gauge potential on arbitrary transverse direction can be generated.

We first consider the case without a magnetic field, for which the low energy Dirac Hamiltonian of the Weyl fermion can be described as follows

$$H = \hbar v_F (\boldsymbol{\sigma} \cdot \boldsymbol{k}) + V_0 = \hbar v_F \left(\sigma_x k_x + \sigma_y k_y + \sigma_z k_z \right) + V_0, \tag{1}$$

where ν_F is the Fermi velocity, and $\boldsymbol{\sigma}$ represents all three Pauli matrices. To investigate the transport properties in the bulk system, we consider Weyl electrons near one node and neglect the contribution of surface states (and hence Fermi arcs) and intervalley scattering to the conduction. By solving the above Hamiltonian, the eigenenergies can be found as $\varepsilon = E_F - V_0 = \pm \hbar v_F k_F$. The positive part of energy represents the electrons carrying negative charge above zero energy while the negative part is for the states that exhibit positively charged behavior (holes) that are unoccupied states in valance band. By considering a transmission of electrons along x-direction at angles γ (the angle between $\boldsymbol{k}$ and the xy plane) and ϕ (the azimuthal angle with respect to the x-axis), the components of the eigenstates of equation (1) can be obtained as

$$\psi_{\pm} \equiv \frac{1}{\sqrt{2}} e^{i\boldsymbol{kr}} \begin{pmatrix} 1 \\ e^{i\phi} \sec\gamma (\pm 1 + \sin\gamma) \end{pmatrix} \equiv \begin{pmatrix} \psi_a \\ \psi_b^{\pm} \end{pmatrix}.$$

The top component of wavefunction ψ_a for incident, propagating and transmitted regions shown in Fig. 1 can be written as

$$\begin{aligned} \Psi_{1,a}(x) &= e^{ik_x x} + r\, e^{-ik_x x}, \quad x < 0, \\ \Psi_{2,a}(x) &= a e^{iq_x x} + b\, e^{-iq_x x}, \quad 0 < x < L, \\ \Psi_{3,a}(x) &= t e^{ik_x x}. \quad x > L. \end{aligned}$$

The next step is to write the bottom component of the wave function ψ_b by using the relation $\psi_2 = e^{i\phi} \sec\gamma (s + \sin\gamma) \psi_1$, where $s = \pm 1$ depending on the sign of energy $(E_F - V_0)$. Assuming the Fermi energy to be always positive, we have

$$\begin{aligned} \Psi_{1,b}(x) &= e^{i\phi} \sec\gamma (1 + \sin\gamma)\, e^{ik_x x} - r e^{-i\phi} \sec\gamma (1 + \sin\gamma) e^{-ik_x x}; \quad x < 0, \\ \Psi_{2,b}(x) &= a e^{i\theta} \sec\alpha (s + \sin\alpha) e^{iq_x x} - b e^{-i\theta} \sec\alpha (s + \sin\alpha) e^{-iq_x x}; \quad 0 < x < L, \\ \Psi_{3,b}(x) &= t\, e^{i\phi} \sec\gamma (1 + \sin\gamma) e^{ik_x x}; \quad x > L. \end{aligned}$$

In the above, the Fermi wavevector is $k_F = \sqrt{k_x^2 + k_y^2 + k_z^2}$ and the three components of wavevector outside of the barrier can be written as $k_x = k_F \cos\gamma \cos\phi$, $k_y = k_F \cos\gamma \sin\phi$, $k_z = k_F \sin\gamma$, while the x-component of wavevector within the barrier is $q_x = \sqrt{\left(\frac{E_F - V_0}{\hbar v_F} \right)^2 - k_y^2 - k_z^2}$. The propagating angles within the barrier $\theta = \tan^{-1}\left(\frac{k_y}{q_x} \right)$ and $\alpha = \tan^{-1}\left(\frac{k_z}{q_x} \cos\theta \right)$ can be found by considering the conservation of the transverse wavevectors k_y and k_z at the barrier interfaces. Finally, the transmission function t can be derived by considering the wavefunction continuity at the barrier interfaces with the proper matching conditions.

Results and Discussions

In Fig. 2, we analyze the transmission probability $T = |t|^2$ in the case of different applied potential V_0 but constant Fermi energy ($E_F \approx 82\,\text{meV}$). The examples (a) and (c) shows the angular dependence of the tunneling probability when V_0 is much greater than E_F, which is the case of electron conductance between electron and hole states at the barrier interface. As shown in (b) and (d), the transmission profile of the system is exactly same as the graphene case presented in ref. 8, if one reduce the system in two-dimension by setting the constant value zero for one of the incident angle ($\gamma = 0$ or $\phi = 0$). The graph (e) shows the case when the V_0 is close to E_F, thus, the Fermi level is very close to the Weyl node in the barrier. Therefore, only normal incident electrons ($\gamma \approx 0$ and $\phi \approx 0$) can be transmitted perfectly.

The additional perfect transmission rings can be understood by the resonance condition of Fermi wavevector k_F and the barrier length L. These perfect transmission angles can be derived by using the relation $q_x L = \pi n$, $n = 0, \pm 1, \ldots$ by substituting the expression of q_x [see Eq. 2 below]. In two-dimensional relativistic materials such as graphene, the consequence of these resonances enables other perfect transmission angles which satisfy the above condition as shown in Fig. 1(b,d) as well as ref. 8. However, here we found perfect transmission rings instead of points as a consequence of these resonances since two incident angles must satisfy the resonance condition in Weyl semimetal. The number and shape of the perfect transmission rings can be intuitively predicted that they are highly dependent on applied voltage and Fermi energy since q_x is a function of V_0 and E_F. Also, it can be clearly seen that larger barrier length must enable more perfect transmission rings as shown in Fig. 3. Moreover, matching of perfect transmission angles in two different transverse direction results in very interesting tunneling profile when the barrier length L is large enough. This can be understood by the combination of many transmission rings caused by incident angles γ and ϕ. Analytically, one can predict these angles by using resonance conditions and wavevectors as

$$L \sqrt{ \frac{(E_F - V_0)^2}{\hbar v_F} - k_F^2 \sin(\gamma)^2 - k_F^2 \cos(\gamma)^2 \sin(\phi)^2 } = \pi\, n, \; n = 0, \pm 1, \ldots \tag{2}$$
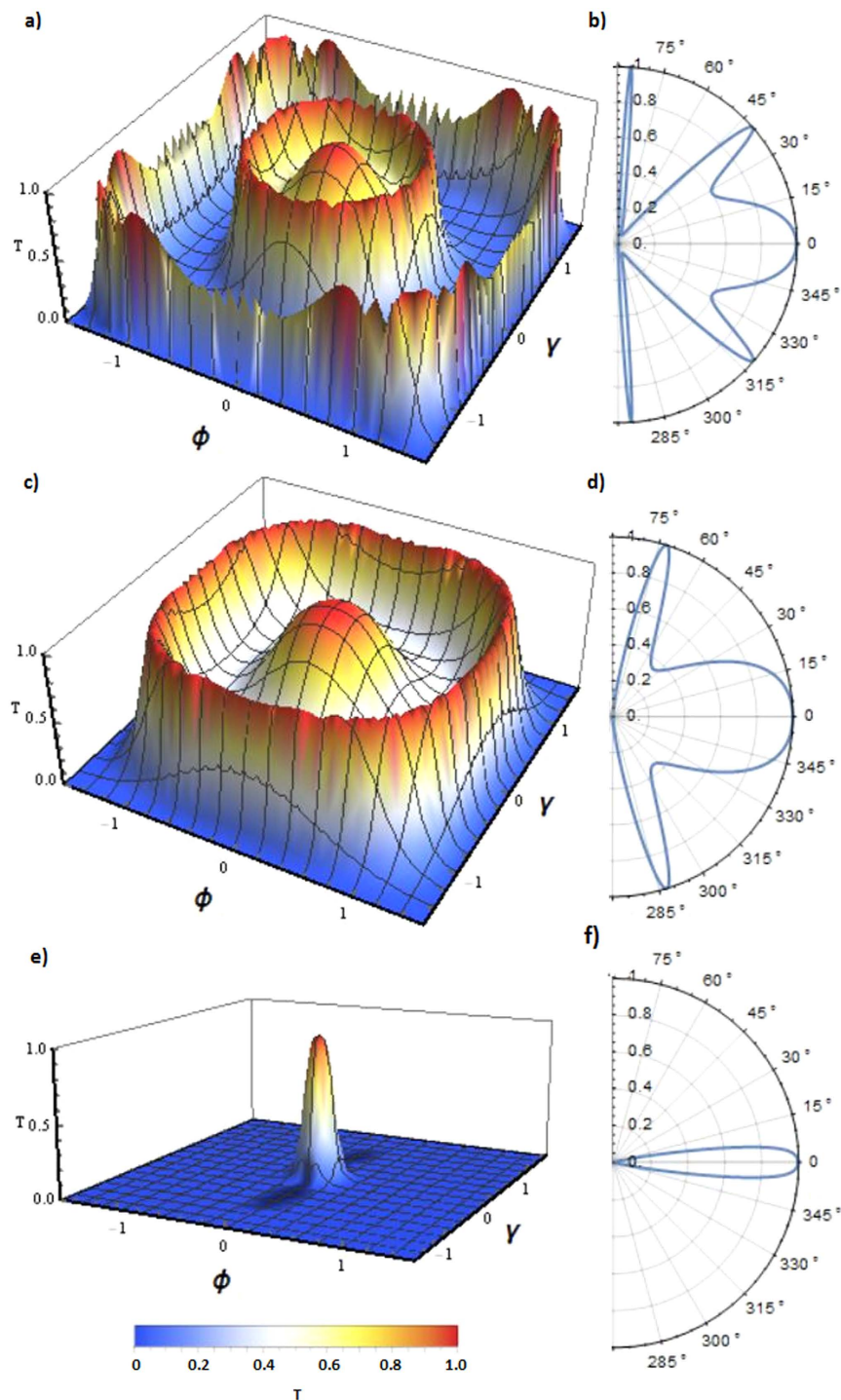
Figure 2. Angular dependence of transmission probability for different configuration of applied potentials in the case of $L = 100\,\text{nm}$ and $E_F \approx 82\,\text{meV}$. (a,c) show the cases of $V_0 \approx 200\,\text{meV}$ and $285\,\text{meV}$ respectively. **(e)** shows that when the applied potential is close to Fermi energy ($V_0 = 80\,\text{meV}$), only normal incidence electrons can transmit as Fermi level is very close to the Weyl node in the barrier region. **(b,d,f)** Represent the cross section of three-dimensional transmissions **(a,c,e)** in the case of $\gamma = 0$.

Every incident angle that satisfies above expression cause a unit transmission probability ($T = 1$) is depicted by bright pixels in Fig. 3. The predicted transmission profiles shown in Fig. 3 may be experimentally observed by using a point electron source and measuring electron transmission density right after the second interface of the barrier.

The absence of normal backscattering has been widely investigated in mostly two-dimensional Dirac semi-metals such as graphene and silicene. It has been revealed that normally incident electrons can be perfectly transmitted even in the case of high applied electrical potentials due to the chiral nature of particles in these materials.
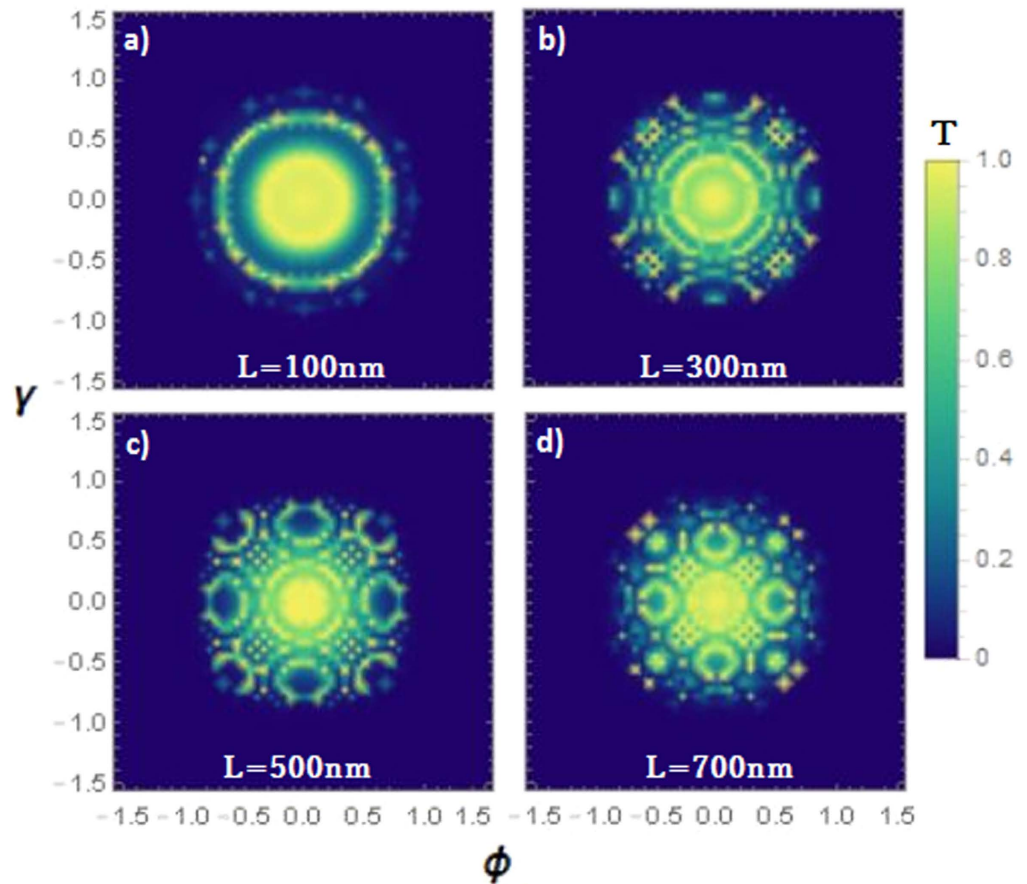
Figure 3. Angular dependence of transmission probability in the case of $E_F \approx 82$ meV, $V_0 = 150$ meV for different configurations of the barrier length L. Larger barrier length results in more magic transmission rings, and the combination of the perfect incident angles for two transverse directions causes different transmission profiles.

This has also been studied in Weyl semimetal multi-barrier structures generated by periodic electrostatic potential gates[30]. Our results on the Klein tunneling transport without a magnetic field also confirm the absence of backscattering and reveal the magic transmission rings, which can be analytically derived from Eq. 2. Besides, it has been shown that the number of magic transmission rings and their configuration are highly dependent on the barrier length [see Fig. 3].

Now, we analyze the transmission profile of Weyl semimetal under the influence of magnetic field induced by ferromagnetic stripes on top and side surfaces. The delta-function magnetic fields at the barrier interfaces cause following gauge potentials on z- and y-directions.

$$\vec{A}_{Bz} = B_{0(z)}\, l_B[\Theta(x) - \Theta(x - L)]\hat{y}$$

$$\vec{A}_{By} = B_{0(y)}\, l_B[\Theta(x) - \Theta(x - L)]\hat{z},$$

where $l_B = \sqrt{\frac{\hbar}{|e|\, B_0}}$. Thus, the Hamiltonian in Equation (1) must be modified as $H = v_F(\boldsymbol{\sigma} \cdot (\boldsymbol{p} + e\boldsymbol{A})) + V_0$. Here, we have neglected the Zeeman splitting since the band shift is very small and only observable under a very high magnetic field of ≈ 25 T, as shown experimentally in the Weyl semimetal TaP[31]. Furthermore, it has been shown that at field strength above 3 T, Weyl semimetals like TaP begin to exhibit insulator-like behavior[31]. The magnetic field causes a change on the both transverse wave vectors as $k_y \rightarrow k_y + \frac{eA_{By}}{\hbar}, k_z \rightarrow k_z + \frac{eA_{Bz}}{\hbar}$. The wave vector along y- and z-direction are recalculated with the contribution of the magnetic field; they can be written as

$$k_y = \frac{E_F \cos\gamma \sin\phi + \eta\, v_F\sqrt{|B_{0(y)}|\,\hbar\,|e|}}{\hbar v_F},$$
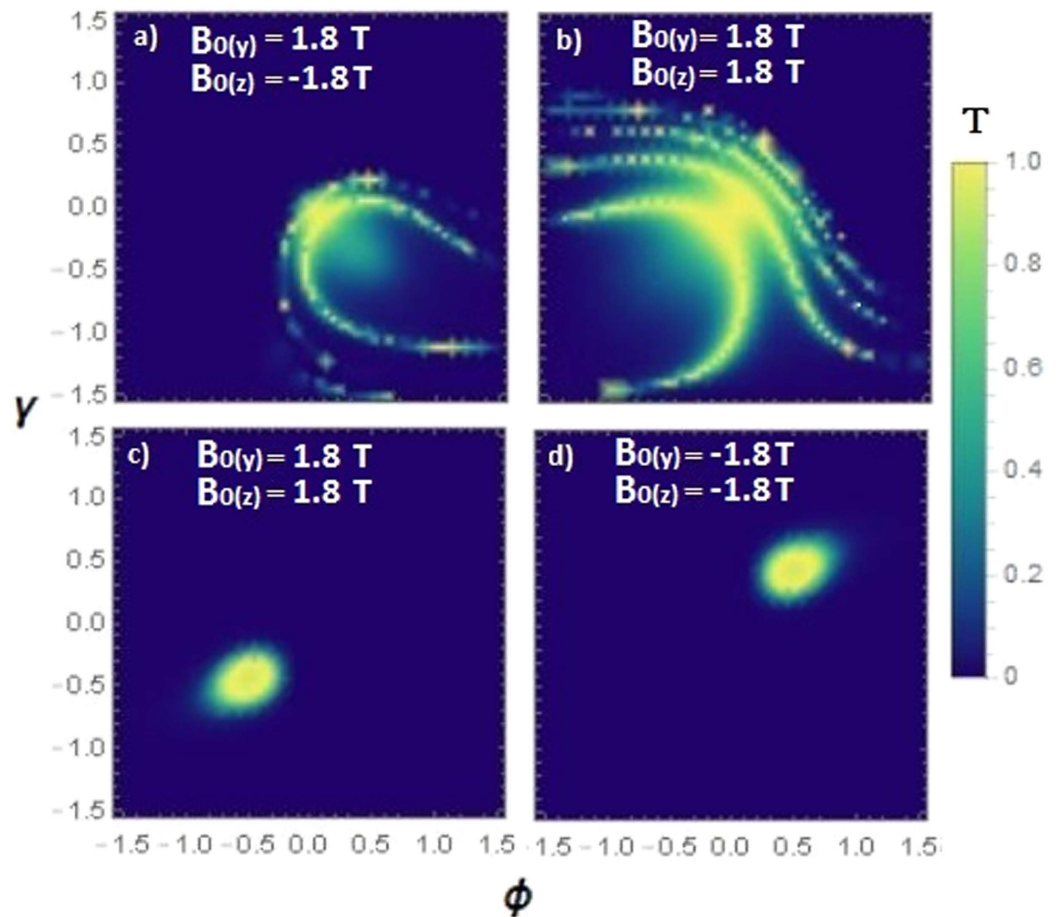
Figure 4. Angular dependence of transmission probability under the influence of magnetic field by considering magnetic gauge potentials on *z*- and y-component of Fermi wavevector for barrier length L = 100 nm. (**a,b**) Shows the effect of magnetic field in the case of $V_0 = 140$ meV and $V_0 = 200$ meV respectively. (**c,d**) Shows the effect of magnetic field on normal incident electrons when the barrier allows only normal incident electrons since the applied potential is close to Fermi energy ($E_F \approx 82$ meV, $V_0 = 60$ meV). It is seen that application of magnetic field can set the perfect transmission angles on the two-dimensional transmission space.

$$k_z = \frac{E_F \sin \gamma + \eta v_F \sqrt{|B_{0(z)}| \, \hbar \, |e|}}{\hbar v_F},$$

where $\eta = \pm 1$ depending on the sign of the magnetic field. Here, the two independent orthogonal magnetic field vectors can create arbitrary angle effective magnetic field that is transverse to the transmission by setting both sign and strength of the magnetic anisotropy of ferromagnetic stripes. Analyzing the angular dependence of the transmission probability, it is shown that electrons are affected by the magnetic field by means of transverse Lorentz displacement. More importantly, a very small range of perfect transmission angles can be selected in two-dimensional transmission space by means of the magnetic gauge potential. Figure 4 shows the effect of magnetic field on the transmission angles and rings. The perfect transmission rings are deflected and distorted in the presence of the magnetic field, as shown in Fig. 4(a) and (b). In the case of normal transmission induced by setting an applied potential close to the Fermi energy [see Fig. 2(e)], the specific wavevector that exhibits absence of backscattering can be tuned by the magnetic gauge potentials. This allows one to generate transmission for a particular incident vector while blocking all other incident vectors. In Fig. 4(c) and (d), the angles corresponding to the absence of backscattering are shifted to different orientations by tuning the magnetic gauge potentials. It can be seen that any point in two-dimensional transmission space can be chosen for unit transmission probability, which may be very useful for electro-optic applications. Moreover, by changing the difference between Fermi energy and barrier height ($E_F - V_0$), the radius of perfect transmission points can be changed as well.

The magnetic barrier profile shown in Fig. 1(b) consists of two asymmetric ferromagnetic strips with an out-of-plane magnetization that give rise to a square-shaped magnetic gauge potential, and is commonly adopted in previous studies on two-dimensional transport under the influence of a magnetic field. For instance, a similar double magnetic barrier structure was considered on the surface of topological insulator[32]. However, ref. 32 also
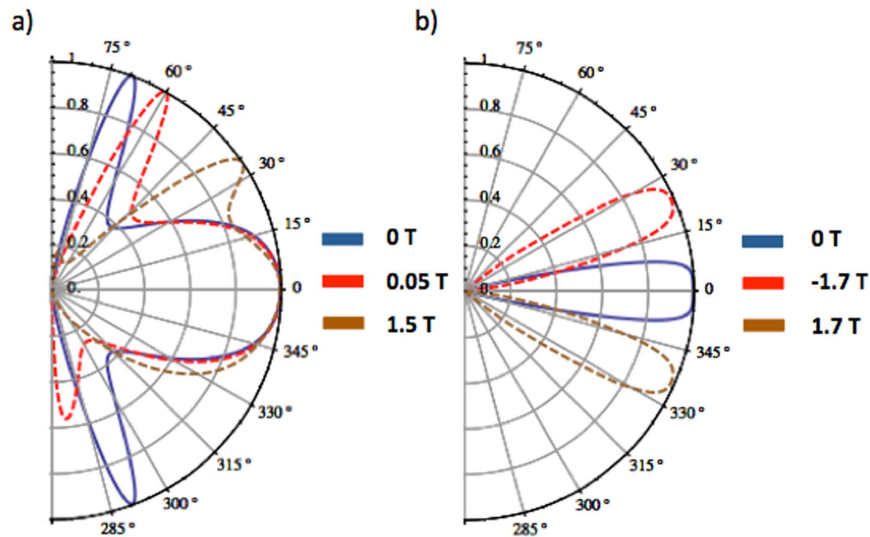
Figure 5. Angular dependence of transmission probability in graphene in the presence of different strength of applied magnetic barrier causing a constant vector potential in the barrier region, and induced by two asymmetric ferromagnetic strips at barrier boundaries for different electrical potential profiles (**a**) 285 meV, and (**b**) 63 meV, where the Fermi energy is 83 meV and barrier length is 100 nm.

considers the case of magnetic field with a square profile, which induces a linearly increasing magnetic gauge potential, as shown in the work. In this case, the resulting Klein tunneling properties would be different since the gauge potential is not constant within the central barrier region. Another option to achieve square shape magnetic vector potential may be using a single ferromagnetic strip whose magnetization is in the in-plane direction[33]. These type of magnetic barriers, i.e., square shape gauge potential, would be useful for electron filtering according to their incident angle when they are combined with another effect (e.g., strain) that can lift the valley or spin degeneracy, as investigated in several previous studies[33–37]. Another work[38] investigates the combined effects of magnetic and electrostatic potential barriers, in either the symmetric or antisymmetric configuration, on the transport properties of graphene. It shows that the symmetric configuration would give rise to a deflection of the incident angle of electrons at the barrier interfaces, which is similar to the predicted Klein tunneling behavior of Weyl semimetals [as depicted in Fig. 4]. On the other hand, the antisymmetric barrier configuration would cause electron collimation closer to the normal direction by reflecting the electrons that possess a large incident angle, or suppression of transmission if electrical potential and Fermi energy are comparable to one another.

Since graphene and Weyl semimetals with the conventional non-tilted energy dispersion have similar energy-momentum relation, the effect of an applied magnetic barrier in the central barrier region in a Weyl semimetal should give rise to similar results to that on the Klein tunneling properties in graphene. Figure 5 confirms that the application of magnetic field on graphene shifts perfect transmission angles, similar to that shown in Fig. 4 for Weyl semimetals, but the former is confined to two dimensions.

The results shown in this paper are obtained by using appropriate parameters that can be realized in current technology. Here, we discuss the validity of the Hamiltonian, and feasibility of electrical and magnetic barrier structures.

The Hamiltonian shown in Eq. 1 describes the dynamics of low energy electrons near one node in Weyl semimetals. Therefore the validity of this approximation is restricted by an energy range depends on the full band structure of the material hosting such a Weyl nodes with linear energy dispersion. Thus far, it has been shown that the linear energy dispersion of Weyl cones along all three directions is effectual up to 0.4 eV in NbAs[17]. Despite this result does not indicate an upper limit, it is larger than the Fermi energy used as example in this work. Moreover, the linear energy dispersion along three directions up to 2.5 eV was also observed in Dirac semimetal Cd_3As_2 which may be driven into Weyl semimetal phase[29].

In our scheme, both electrostatic and magnetic barrier exist. To generate such an electrostatic barriers (p-n-p), we require modulation of the carrier concentration of the sample as a whole, as well as modulation of the carrier concentration only within the barrier region. One of the methods to achieve this is by using a back gate to change the carrier concentration of the whole sample, thus causing a change of the Fermi level, and a top gate to change the carrier concentration within only the gated (barrier) region. The validity of this method in three-dimensional semimetals has been experimentally confirmed in Cd_3As_2 by the observation of a gate-tunable Fermi level and carrier concentration[28]. Another method to generate an electrostatic barrier is modulating the doping concentration in three regions. In particular, tuning of the carrier concentration by alkali doping has been achieved in Cd_3As_2, where the Fermi level has been raised to approximately 250 meV above the Dirac point[29].

Based on current nanotechnology, magnetic barriers may be realized by several different methods. One method is by fabricating ferromagnetic stripes on the top of the structure[39–45], which we used as an example in this manuscript. Another option of achieving the spatial modulation of the magnetic field is by depositing a superconductor film with the desired pattern on top of the device structure, and then applying a uniform

magnetic field[42,46,47]. Various structures of magnetic barriers have been experimentally achieved by using these methods. The upper limit of the magnetic field strength induced by ferromagnetic stripes directly depends on the saturation magnetization of the ferromagnetic material. For instance, the saturation magnetization of magnetic barrier around 3.75 T has been experimentally achieved, and the transport properties under the influence of the resulting magnetic barrier have been investigated in two-dimensional electron gas structures[39]. The upper limit of the magnetic barrier strength induced by a uniform magnetic field on superconductor pattern is restricted by the critical magnetization of the superconductor material, which is in excess of 30 T, as shown in Nb_3Sn[48].

Although we focused on a single magnetic barrier which induces a constant gauge potential within the barrier region [see Fig. 1(b)], it has been shown (see e.g., refs 49 and 50) that magnetic barrier superlattice of two-dimensional Dirac semimetals (such as graphene) can also yield very interesting results, as far as the electron collimation and resonant tunneling properties are concerned. The origin of the shift of the electron's momentum (shown in Fig. 4) can be understood by the mismatch of the Fermi surfaces along the transmission direction. In the case of magnetic superlattices, the mismatch is cumulative through the lattice, and can induce distinct transmission profiles depending on the structure of superlattice. If the resulting magnetic gauge potential profiles are square-shaped and antisymmetric, they tend to lead to electron collimation towards normal incidence by reflecting the electrons having large incident angles, as shown in graphene previously[49]. This is unlike the results plotted in Fig. 4, which show an asymmetric transmission with respect to normal incidence. In the case of a superlattice consisting a periodic square-shaped magnetic field profile, the resulting gauge potential has a zig-zag characteristic, which in turn, causes a zig-zag displacement of the Fermi surfaces of Weyl fermions in **k**-space. Therefore, additional resonances may be expected depending on the number of periods of the superlattice[50]. Additionally, the conductance exhibits an oscillatory behavior with respect to the Fermi energy[50]. As compared to our results, such a magnetic superlattice structure may potentially induce additional magic transmission rings in the transmission profile.

Conclusion

Thus far, the Klein tunneling has been widely investigated in graphene and successfully realized by direct and indirect measurements[9,10]. Experimental realization of Weyl semimetal has made possible this kind of relativistic tunneling in three-dimension as well. Since the direct evidence of Klein tunneling requires the application of magnetic field to observe the phase shift of conductance oscillations[10], we investigated the tunneling properties and angular dependence of the transmission under the influence of magnetic field with experimentally feasible methods and parameters. The results showed very interesting transmission profiles such as perfect transmission rings due to the resonance conditions. The effect of barrier length on the angular dependence of transmission profile results in an interesting transmission profile due to perfect transmission angles of the combination of two transverse directions. By using a point electron source, these transmission profiles can be experimentally observed by measuring the electron transmission density on the second interface of the potential barrier. In addition, we also analyzed the magic transmission rings in Weyl semimetals as a function of applied potentials and barrier widths. By tuning the potential barrier height, magic transmission rings can be controlled and used for many applications such as electron collimation[51] and Veselago lens[52–54] for electrons in three-dimensional systems. It has been shown previously that the application of asymmetric potential barriers may suppress the magic transmission peaks in graphene[11]. Therefore, further analysis of the magic transmission rings in Weyl semimetals may help realize the transistor effect in such materials. Finally, we showed that the perfect transmission regions can be selected by tuning the magnetic fields which may be used to generate localized transmission in the bulk of Weyl semimetals, a prediction which may be utilized in electro-optic applications.

References

1. Calogeracos, A. & Dombey, N. History and physics of the Klein paradox. *Contemp. Phys.* **40,** 313 (1999).
2. Dombey, N. C., A. Seventy years of the Klein paradox. *Phys. Rep.* **315,** 41 (1999).
3. Greiner, W., Mueller, B. & Rafelski, J. *Quantum Electrodynamics of Strong Fields*. Springer, Berlin (1985).
4. Grib, A. A., Mamayev, S. G. & Mostepanenko, V. M. Vacuum Fields in Strong Fields. *Friedmann, St-Petersburg* (1994).
5. Klein, O. Discrete Symmetry in Relativistic Quantum Mechanics. *Z. Phys.* **53,** 157 (1929).
6. Krekora, P., Su, Q. & Grobe, R. Klein Paradox in Spatial and Temporal Resolution. *Phys. Rev. Lett.* **92,** 040406 (2004).
7. Novoselov, K. S. *et al.* Electric Field Effect in Atomically Thin Carbon Films. *Science* **306,** 666–669 (2004).
8. Katsnelson, M. I., Novoselov, K. S. & Geim, A. K. Chiral tunnelling and the Klein paradox in graphene. *Nature Physics* **2,** 620–625 (2006).
9. Stander, N., Huard, B. & Goldhaber-Gordon, D. Evidence for Klein Tunneling in Graphene p-n Junctions. *Phys. Rev. Lett.* **102,** 026807 (2009).
10. Young, A. F. & Kim, P. Quantum interference and Klein tunnelling in graphene heterojunctions. *Nat Phys* **5,** 222–226 (2009).
11. Kleptsyn, V., Okunev, A., Schurov, I., Zubov, D. & Katsnelson, M. I. Chiral tunneling through generic one-dimensional potential barriers in bilayer graphene. *Phys. Rev. B* **92,** 165407 (2015).
12. Reijnders, K., Tudorovskiy, T. & Katsnelson, M. Semiclassical theory of potential scattering for massless Dirac fermions. *Annals of Physics* **333,** 155–197 (2013).
13. Tudorovskiy, T., Reijnders, K. J. A. & Katsnelson, M. I. Chiral tunneling in single-layer and bilayer graphene. *Physica Scripta* **2012,** 014010 (2012).
14. Bala Kumar, S., Jalil, M. B. A. & Tan, S. G. Klein tunneling in graphene systems under the influence of magnetic field. *Journal of Applied Physics* **114,** 084314 (2013).
15. Lv, B. Q. *et al.* Experimental Discovery of Weyl Semimetal TaAs. *Physical Review X* **5,** 031013 (2015).
16. Lv, B. Q. *et al.* Observation of Weyl nodes in TaAs. *Nature Physics* **11,** 724 (2015).
17. Xu, S.-Y. *et al.* Discovery of a Weyl fermion state with Fermi arcs in niobium arsenide. *Nature Physics* **11,** 748 (2015).
18. Young, S. M. *et al.* Dirac Semimetal in Three Dimensions. *Phys. Rev. Lett.* **108,** 140405 (2012).
19. Xu, N. *et al.* Observation of Weyl nodes and Fermi arcs in tantalum phosphide. *Nature Communications* **7,** 11006 (2016).
20. Xu, S.-Y. *et al.* Discovery of a Weyl fermion semimetal and topological Fermi arcs. *Science* **349,** 613–617 (2015).

21. Xu, S.-Y. *et al.* Observation of Fermi arc surface states in a topological metal. *Science* **347,** 294–298 (2015).
22. Borisenko, S. *et al.* Time-Reversal Symmetry Breaking Type-II Weyl State in YbMnBi2. *arXiv:1507.04847* (2015).
23. Hosur, P. & Qi, X. Recent developments in transport phenomena in Weyl semimetals. *Comptes Rendus Physique* **14,** 857–870 (2013).
24. Parameswaran, S. A., Grover, T., Abanin, D. A., Pesin, D. A. & Vishwanath, A. Probing the Chiral Anomaly with Nonlocal Transport in Three-Dimensional Topological Semimetals. *Physical Review X* **4,** 031035 (2014).
25. Hosur, P., Parameswaran, S. A. & Vishwanath, A. Charge Transport in Weyl Semimetals. *Phys. Rev. Lett.* **108** (2012).
26. Ramakrishnan, N., Milletari, M. & Adam, S. Transport and magnetotransport in three-dimensional Weyl semimetals. *Phys. Rev. B* **92,** 245120 (2015).
27. Shekhar, C. *et al.* Extremely large magnetoresistance and ultrahigh mobility in the topological Weyl semimetal candidate NbP. *Nature Physics* **11,** 645 (2015).
28. Liu, Y. *et al.* Gate-tunable quantum oscillations in ambipolar Cd3As2 thin films. *Npg Asia Materials* **7,** e221 (2015).
29. Liu, Z. K. *et al.* A stable three-dimensional topological Dirac semimetal Cd3As2. *Nature Materials* **13,** 677–681 (2014).
30. Bai, C. X., Yang, Y. L. & Chang, K. Chiral tunneling in gated inversion symmetric Weyl semimetal. *Scientific Reports* **6,** 15 (2016).
31. Hu, J. *et al.* π Berry phase and Zeeman splitting of Weyl semimetal TaP. *Scientific Reports* **6,** 18674 (2016).
32. Wu, Z., Peeters, F. M. & Chang, K. Electron tunneling through double magnetic barriers on the surface of a topological insulator. *Phys. Rev. B* **82,** 115211 (2010).
33. Zhai, F., Zhao, X., Chang, K. & Xu, H. Q. Magnetic barrier on strained graphene: A possible valley filter. *Phys. Rev. B* **82,** 115442 (2010).
34. Fujita, T., Jalil, M. B. A. & Tan, S. G. Valley filter in strain engineered graphene. *Appl. Phys. Lett.* **97,** 3 (2010).
35. Yesilyurt, C., Tan, S. G., Liang, G. & Jalil, M. B. A. Efficient dual spin-valley filter in strained silicene. *Applied Physics Express* **8,** 105201 (2015).
36. Yesilyurt, C., Tan, S. G., Liang, G. C. & Jalil, M. B. A. Perfect valley filter in strained graphene with single barrier region. *Aip Advances* **6,** 056303 (2016).
37. Soodchomshom, B. Perfect spin-valley filter controlled by electric field in ferromagnetic silicene. *Journal of Applied Physics* **115,** 023706 (2014).
38. Zhai, F. & Chang, K. Theory of huge tunneling magnetoresistance in graphene. *Phys. Rev. B* **77,** 113409 (2008).
39. Cerchez, M., Hugger, S., Heinzel, T. & Schulz, N. Effect of edge transmission and elastic scattering on the resistance of magnetic barriers: Experiment and theory. *Phys. Rev. B* **75,** 035341 (2007).
40. Hong, J. *et al.* Local Hall effect in hybrid ferromagnetic/semiconductor devices. *Appl. Phys. Lett.* **90,** 023510 (2007).
41. Kubrak, V. *et al.* Magnetoresistance of a two-dimensional electron gas due to a single magnetic barrier and its use for nanomagnetometry. *Appl. Phys. Lett.* **74,** 2507–2509 (1999).
42. Matulis, A., Peeters, F. M. & Vasilopoulos, P. Wave-vector-dependent tunneling through magnetic barriers. *Phys. Rev. Lett.* **72,** 1518–1521 (1994).
43. Nogaret, A., Bending, S. J. & Henini, M. Resistance Resonance Effects through Magnetic Edge States. *Phys. Rev. Lett.* **84,** 2231–2234 (2000).
44. Nogaret, A., Lawton, D. N., Maude, D. K., Portal, J. C. & Henini, M. Hall anomaly of diffusive magnetic waveguides. *Phys. Rev. B* **67,** 165317 (2003).
45. Vančura, T. *et al.* Electron transport in a two-dimensional electron gas with magnetic barriers. *Phys. Rev. B* **62,** 5074–5078 (2000).
46. Bending, S. J., von Klitzing, K. & Ploog, K. Weak localization in a distribution of magnetic flux tubes. *Phys. Rev. Lett.* **65,** 1060–1063 (1990).
47. Carmona, H. A. *et al.* Two Dimensional Electrons in a Lateral Magnetic Superlattice. *Phys. Rev. Lett.* **74,** 3009–3012 (1995).
48. Godeke, A. A review of the properties of Nb3Sn and their variation with A15 composition, morphology and strain state. *Superconductor Science and Technology* **19,** R68 (2006).
49. Sankalpa, G. & Manish, S. Electron optics with magnetic vector potential barriers in graphene. *Journal of Physics: Condensed Matter* **21,** 292204 (2009).
50. Quan-Sheng, W., Sheng-Nan, Z. & Shi-Jie, Y. Transport of the graphene electrons through a magnetic superlattice. *Journal of Physics: Condensed Matter* **20,** 485210 (2008).
51. Park, C.-H., Son, Y.-W., Yang, L., Cohen, M. L. & Louie, S. G. Electron Beam Supercollimation in Graphene Superlattices. *Nano Letters* **8,** 2920–2924 (2008).
52. Cheianov, V. V., Fal'ko, V. & Altshuler, B. L. Focusing of Electron Flow and a Veselago Lens in Graphene. *Science* **315,** 1252–1255 (2007).
53. Gupta, G., Jalil, M. B. A., Yu, B. & Liang, G. Performance evaluation of electro-optic effect based graphene transistors. *Nanoscale* **4,** 6365–6373 (2012).
54. Lee, G.-H., Park, G.-H. & Lee, H.-J. Observation of negative refraction of Dirac fermions in graphene. *Nat Phys* **11,** 925–929 (2015).

Acknowledgements

Author Contributions

C.Y. developed the idea and performed the analytical and numerical calculations. The obtained results were discussed with S.G.T., G.L. and M.B.A.J., C.Y. and M.B.A.J. wrote the manuscript. All the authors contributed to interpretation and discussion of obtained results and commented on the manuscript.

Additional Information